

1 Crustal structure beneath Montserrat, Lesser Antilles, constrained by xenoliths,  
2 seismic velocity structure and petrology

3

4 Kiddle, E.J.<sup>1</sup>, B. Edwards<sup>2</sup>, S.C. Loughlin<sup>3</sup>, M. Petterson<sup>4</sup>, R.S.J. Sparks<sup>1</sup>, B. Voight<sup>5</sup>.

5

6 1. Department of Earth Sciences, University of Bristol, Wills Memorial Building,

7 Queen's Road, Bristol, BS8 1RJ, UK.

8 2. Department of Geology, Dickinson College, Carlisle, PA 17013-2896, USA.

9 3. British Geological Survey, Murchison House, West Mains Road, Edinburgh, EH9

10 3LA, UK.

11 4. Department of Geology, University of Leicester, Leicester LE1 7RH4, UK.

12 5. Department of Geosciences, Pennsylvania State University, PA 16802.

13

13 **Abstract**

14 Noritic anorthosite, gabbroic anorthosite and hornblende-gabbro xenoliths are  
15 ubiquitous in the host andesite at Montserrat. Other xenoliths include quartz diorite,  
16 metamorphosed biotite-gabbro, plagioclase-hornblendite and plagioclase-  
17 clinopyroxenite. Mineral compositions suggest a majority of the xenoliths are  
18 cognate. Cumulate, hypabyssal and crescumulate textures are present. A majority of  
19 the xenoliths are estimated to have seismic velocities of 6.7-7.0 km/s for vesicle-free  
20 assemblages. These estimates are used in conjunction with petrological models to help  
21 constrain the SEA CALIPSO seismic data and the structure of the crust beneath  
22 Montserrat. Andesitic upper crust is interpreted to overlie a lower crust dominated by  
23 amphibole and plagioclase. Xenolith textures and seismic data indicate the presence  
24 of hypabyssal intrusions in the shallow crust. The structure of the crust is consistent  
25 with petrological models indicating that fractionation is the dominant process  
26 producing andesite at Montserrat.

27

27 **Introduction**

28 The composition of arc crust is a fundamental issue in earth sciences. Seismic surveys  
29 suggest that arcs are significantly thicker than oceanic crust, with inferred  
30 compositions more mafic than continental crust (e.g. Christensen and Mooney, 1995).  
31 Most of our knowledge derives from seismic surveys, exhumed crustal sections and  
32 crustal xenoliths. Here igneous xenoliths sampled from andesite lavas on Montserrat  
33 are described and used, together with petrological information, to help interpret  
34 seismic velocity data obtained from the SEA CALIPSO project. Together these data  
35 constrain the crustal structure beneath Montserrat.

36

37 **Background**

38 Montserrat is located in the Lesser Antilles island arc related to subduction of the  
39 Atlantic plate beneath the Caribbean plate. Arc volcanism has been active since the  
40 Cretaceous and shifted westward during the Miocene, producing a double island  
41 chain. Early seismic surveys determined an average crustal thickness in the Lesser  
42 Antilles of ~30km, with a heterogeneous upper crust ( $V_p=6.2\text{km/s}$ ) of variable  
43 thickness, and a higher velocity lower crust ( $V_p=6.9\text{km/s}$ , Westbrook and McCann,  
44 1986; and references therein). However Christeson et al. (2008) reported an average  
45 crustal thickness of 24km.

46

47 The four volcanic centres of Montserrat date back to 2.6Ma (Harford et al., 2002).  
48 The current eruption of Soufrière Hills Volcano (SHV) began in 1995, characterised  
49 by phases of dome growth and collapse. Deposits include andesitic domes and  
50 pyroclastic, lahar and debris avalanche deposits. Andesite is the dominant rock type.  
51 Evidence from deformation studies (Mattioli et al., 1998) and melt inclusions (Devine

52 et al., 1998) indicate a magma chamber at 5-6km depth beneath the SHV. A deeper  
53 chamber (~12km) has been inferred from deformation modelling combined with  
54 magma extrusion volumes (Elsworth et al., 2008). Mafic magmatic inclusions in the  
55 host andesite suggest repeated input of basalt and basaltic andesite magma  
56 accompanied by reheating (e.g. Sparks et al., 1998; Murphy et al., 1998).

57

## 58 **Methodology**

59 Crustal xenoliths were collected from all four volcanic centres. Modal mineral  
60 proportions were obtained for a representative selection of xenoliths, host andesite  
61 and mafic magmatic inclusions by point counting using a petrographic microscope.  
62 Mineral phases were analysed for major elements using the Cameca SX100 electron  
63 microprobe at Bristol University with a 20kV accelerating voltage and 10nA beam  
64 current. Textures were analysed using a petrological microscope and the Scanning  
65 Electron Microscope (SEM).

66

67 The seismic velocity of a rock can be estimated from modal proportions and elastic  
68 properties of individual minerals, assuming isotropic fabrics, using the following  
69 equation:

$$70 \quad M^* = \left( \sum_{i=1}^n (v_i M_i)^t \right)^{\frac{1}{t}}$$

71

72 where  $M^*$  is the bulk or shear modulus of the composite;  $v_i$  is the volumetric  
73 proportion of the  $i$ th mineral; and  $M_i$  is the bulk or shear modulus of the  $i$ th mineral.

74 The Voigt average ( $M_V$ ) assumes uniform strain ( $t=1$ ) and the Ruess average ( $M_R$ )

75 assumes uniform stress ( $t=-1$ ) throughout the polymineralic rock (Watt et al., 1976,

76 and references therein). These averaging schemes effectively provide upper and lower  
77 bounds, therefore the arithmetic mean  $(M_V+M_R)/2$ , or the ‘Hill average’, is commonly  
78 used (Watt et al., 1976). Unless stated otherwise, quoted velocities have been  
79 calculated using the arithmetic mean. Elastic constants were taken from the  
80 compilation of Hacker and Abers (2004; and references therein). Average mineral  
81 compositions from electron probe analyses were used to extrapolate between end-  
82 member elastic constants, except for plagioclase (Angel et al., 2004). The effect of  
83 porosity on seismic velocities can be estimated using the equation below (Wyllie et  
84 al., 1958):

$$86 \quad \frac{1}{V} = \frac{\phi}{V_f} + \frac{1-\phi}{V_m}$$

87

88 where  $\phi$  is fractional porosity,  $V_f$  and  $V_m$  are the seismic velocities of the pore fluid  
89 and the rock matrix respectively.

90

91 Bulk rock temperature and pressure corrections of  $-0.0005 \text{ km/s } ^\circ\text{C}^{-1}$  (Christensen,  
92 1979) and  $0.006 \text{ s}$  (Rudnick and Fountain, 1995) respectively were used. Velocities  
93 were modelled based on a normal arc geothermal gradient of  $30 \text{ }^\circ\text{C/km}$ . Calculated  
94 velocity gradients of most rock types compare well to estimates based on temperature  
95 and pressure derivatives of individual mineral elastic constants (Hacker and Abers,  
96 2004), with a maximum discrepancy of  $0.09 \text{ km/s}$  at  $20\text{km}$  depth.

97

## 98 **Results and Discussion**

99

### 100 **Xenoliths**

101 Most xenoliths are intrusive igneous rocks. They can be classified as: noritic  
102 anorthosites, gabbroic anorthosites, and hornblende-gabbros. Other less common  
103 xenoliths include: quartz diorite, metamorphosed biotite-gabbro, and nearly pure (80-  
104 86%) monomineralic rocks including: plagioclase-hornblendite and plagioclase-  
105 clinopyroxenite. Xenolith modal mineralogy is characterised by varying proportions  
106 of plagioclase, amphibole, orthopyroxene, clinopyroxene, titanomagnetite, ilmenite  
107 and quartz, similar to mineral assemblages in the host andesite (Table 1). Montserrat  
108 xenoliths have similar mineral assemblages to xenoliths found throughout the Lesser  
109 Antilles (Arculus and Wills, 1980), apart from the absence of olivine.

110

111 The xenoliths are mostly unlayered and isotropic. Sharp contacts with the host  
112 andesite and absence of chilled margins suggest the xenoliths were largely or entirely  
113 consolidated prior to entrainment, in contrast to the mafic magmatic inclusions  
114 (Figure 1). Many of the xenoliths have orthocumulate textures with vesiculated  
115 groundmasses (<26vol%) and abundant plagioclase microlites, similar to xenoliths  
116 from other Antilles islands (Arculus and Wills, 1980). This indicates the presence of  
117 partially quench crystallized interstitial melt (<42%). Mirolitic cavities partially  
118 infilled with secondary cristobalite together with the fine-medium grain size indicate  
119 that most xenoliths crystallised in hypabyssal intrusions. Some samples display  
120 adcumulate and crescumulate textures. One sample consists of alternating pyroxene-  
121 anorthosite and plagioclase-clinopyroxenite layers, with crescumulate textures normal  
122 to the mineral layering. Such textures are interpreted as rapid crystal growth from a  
123 supercooled melt at the margins of a magma body (e.g. Donaldson, 1977).

124

125 Plagioclase compositions of most xenoliths ( $An_{46-91}$ ) show similar variation to the  
126 host andesite and mafic inclusions (Murphy et al., 1998). Crystals display normal,  
127 reverse and oscillatory zoning consistent with repeated injections of mafic magma, as  
128 interpreted for the host andesite (e.g. Sparks et al., 1998; Murphy et al., 1998). Sodic  
129 plagioclase microlites ( $An_{20-37}$ ) are consistent with crystallisation from a late-stage  
130 melt.

131

132 Mafic phases include clinopyroxene ( $En_{37-40}Wo_{38-45}$ )  $\pm$ orthopyroxene ( $En_{54-60}Wo_{2-4}$ )  
133  $\pm$ magnesio-hornblende (Leake et al., 1997). No significant core-rim variations are  
134 observed in a majority of the xenoliths. Hornblende typically contains 6.3-8.8wt%  
135  $Al_2O_3$ , with magnesium numbers of 58-64, a similar range to the host andesite  
136 (Murphy et al., 1998). A few xenoliths have more Al-rich hornblende similar to the  
137 mafic inclusions (<14wt%  $Al_2O_3$ ; Murphy et al., 1998). Similar mineral compositions  
138 of most xenoliths to the host andesite suggest they are cognate (or there is a primary  
139 magmatic relationship). The lack of suitable mineral assemblages has hindered  
140 estimates of xenolith equilibration pressures.

141

142 Hornblende from plagioclase-hornblendite has significantly higher magnesium  
143 numbers of 70-76. The layered sample is compositionally distinct, with highly calcic  
144 plagioclase ( $An_{79-87}$ ) and a small proportion of more magnesium-rich orthopyroxene  
145 ( $En_{65-67}$ ). Sodic plagioclase rims ( $An_{36-64}$ ) and Fe-rich orthopyroxene rims ( $En_{46-52}$ ) are  
146 present in the pyroxene-anorthosite layer. This sample is interpreted as crystallization  
147 at the margins of a mafic magma body, with rim compositions indicative of  
148 infiltration of the crystal mush by more evolved melts.

149

150 **Velocity estimates**

151 Velocity estimates of the xenoliths are very similar despite the range of mineral  
152 assemblages (Figure 2). Velocity of most xenoliths calculated from their primary  
153 modal mineralogy show good correlation with laboratory measurements of similar  
154 rocks (Table 1; Christensen and Mooney, 1995). However calculated velocities of the  
155 andesite and mafic magmatic inclusions are significantly higher. Alteration minerals  
156 and a small proportion of glass observed in these rocks may produce some of this  
157 variation.

158

159 Velocities have been calculated based on three scenarios: (1) no vesicles, assuming  
160 that vesicles are only abundant in the shallow crust; (2) all vesicles are filled with  
161 water; and (3) all vesicles are filled with secondary quartz, based on observed  
162 cristobalite (Figure 2). Water-saturated vesicles dramatically reduce seismic velocity  
163 estimates by up to 2.9 km/s for the highly vesicular samples. Secondary quartz  
164 reduces velocities by <0.3 km/s.

165

166 **SEA CALIPSO results**

167 The upper crust beneath Montserrat is considered to consist largely of andesite based  
168 on surface geology and our new observations of xenoliths formed in shallow  
169 intrusions. An intrusive complex could explain the high velocity core beneath the  
170 island imaged by the SEA CALIPSO project (Paulatto et al., in press; Shalev et al.,  
171 this issue). The calculated seismic velocity of andesite is much higher pore-free than  
172 observed velocities, indicating that porosity is an important control of velocity in the  
173 uppermost crust (0-5km). Field observations indicate that volcanoclastic rocks likely  
174 dominate the near-surface, with primary and secondary porosity from vesicles and

175 inter-particle spaces. At the greatest resolvable depth (~8km; Paulatto et al., in press)  
176 seismic tomography results are lower than all calculated pore-free velocities.

177

178 Sevilla et al. (subjudice) have produced a receiver function profile that resolves the  
179 Moho at ~30km depth. A mid-crustal layer ~1km thick with velocities of 6.0-6.7 km/s  
180 is consistent with measured (Christensen and Mooney, 1995) and calculated velocities  
181 of quartz diorite. Lower crustal velocities of 6.7-7.0 km/s (Sevilla et al., subjudice)  
182 match estimated velocities of plagioclase-hornblendite and basaltic to basaltic  
183 andesite mafic inclusions, and measured velocities of gabbro, norite, anorthosite and  
184 hornblendite (Figure 3; Christensen and Mooney, 1995). Relict oceanic crust may also  
185 be present in the lower crust.

186

### 187 **Constraints from petrology**

188 Several igneous processes can lead to layering of island arc crust, including partial  
189 melting of older crust and crystallisation of basalt, together with segregation of  
190 residual evolved melts. These scenarios produce physically similar layering with more  
191 differentiated magma supplied to the upper crust leaving denser more mafic  
192 cumulates or restite in the lower crust (Annen et al., 2006). Thus it is difficult to  
193 distinguish between these processes from seismic velocity data alone.

194

195 Magmatic parents to the andesite magma could be represented by the mafic inclusions  
196 or the South Soufrière Hills basaltic andesite. Zellmer et al. (2003) calculated that the  
197 most evolved mafic inclusion could be produced from the least evolved mafic  
198 inclusion by fractional crystallisation of 49% amphibole and 21% plagioclase. A  
199 further ~10% crystallisation is necessary to produce the Th concentration of the most

200 evolved andesite. The andesite can also be modelled by 65% crystallisation of  
201 plagioclase and amphibole from the least evolved South Soufrière Hills lava (Zellmer  
202 et al., 2003).

203

204 Fractionation models (Zellmer et al., 2003) thus imply that an andesitic upper crust  
205 should be complemented by cumulates of plagioclase and amphibole in the lower  
206 crust. Upper/middle crust interpreted from the receiver function profile (Sevilla et al.,  
207 subjudice) is ~10km thick to the island surface, and lower crust is ~21km thick. The  
208 ratio of upper to lower crust is therefore 1:2. This is consistent with the 65% South  
209 Soufrière Hills fractionation model (Zellmer et al., 2003). Without a 3D velocity  
210 structure we cannot account for the lateral extent of crustal layers. Assuming the  
211 lower crust dominantly comprises plagioclase and amphibole, observed seismic  
212 velocities (Sevilla et al., subjudice) correspond to 30-80% hornblende and  
213 corresponding plagioclase. These fractionation models are based on a parental magma  
214 that is evolved with respect to primitive melts. Therefore additional cumulates of  
215 pyroxene, olivine and plagioclase are either present in the lower crust or beneath the  
216 petrological Moho, noting that the velocities of these ultramafic cumulates could be  
217 >7.7 km/s.

218

219 Some evidence indicates that the andesite is at least partially produced by anatexis.  
220 Stable isotope ratios of amphiboles (Harford and Sparks, 2001) and bulk U/Th ratios  
221 indicate partial melting and remobilisation of previous intrusions (Zellmer et al.,  
222 2003). Tatsumi et al. (2008) suggest that ~30% melting of basaltic crust could  
223 produce andesitic magma. This would produce a middle to lower crust ratio of 1:2  
224 also similar to the observed crustal structure. Oxygen isotopes are consistent with a

225 contribution of 10-20% hydrothermally altered crust. However trace element  
226 concentrations can largely be modelled by fractional crystallisation (Zellmer et al.,  
227 2003). The presence of cumulate textured xenoliths, together with petrological and  
228 geochemical evidence, favours a dominant role of intrusion and fractionation of  
229 incremental additions of basalt in the model of arc crust formation at Montserrat.

230

### 231 **Conclusion**

232 Igneous xenoliths are present in the host lavas at Montserrat, with cumulate and  
233 hypabyssal textures. Most have mineral assemblages and mineral compositions  
234 indicating that they represent hypabyssal intrusive equivalents of the andesite, or  
235 cumulate rocks formed by fractionation of basaltic andesite and andesite. The  
236 presence of partially infilled vesicles in most xenoliths indicates shallow  
237 crystallisation. Surface geology and seismic velocities (Paulatto et al., in press) are  
238 most consistent with an upper crust composed of andesitic volcanic and related  
239 intrusive rocks. The xenoliths and fast velocity regions beneath the volcanic centres of  
240 Montserrat (Paulatto et al., in press; Shalev et al., this issue) support the interpretation  
241 of intrusive complexes. Petrological models (Zellmer et al., 2003) suggest the lower  
242 crust contains cumulate rocks dominated by amphibole and plagioclase, which is  
243 consistent with seismic velocities (Sevilla et al., subjudice). The proportion of upper  
244 intermediate crust to cumulate or restitic lower crust indicates that andesite has been  
245 produced by fractionation of the South Soufrière Hills lava (Zellmer et al., 2003) or  
246 partial melting of an initial basaltic crust (Tatsumi et al., 2008). A model of arc crust  
247 formation largely by fractionation is consistent with xenoliths, petrology and the SEA  
248 CALIPSO seismic velocity data.

249

250 **Acknowledgements**

251 This work is funded by the Natural Environment Research Council and the British  
252 Geological Survey. EJK acknowledges Natalie Starkey, Amy Dabrowa and the  
253 Montserrat Volcano Observatory for help in the field. EJK also thanks Stuart Kearns  
254 for help with EMPA analyses and Richard Arculus for useful discussion. RSJS  
255 acknowledges support of a European Research Council Advanced grant.

256

256 **References**

- 257 Angel, R. (2004), Equations of state of plagioclase feldspars, *Contrib. Mineral.*  
258 *Petrol.*, 146(4), doi: 10.1007/s00410-003-0515-5.
- 259 Annen, C., J.D. Blundy and R.S.J. Sparks (2006), The Genesis of Intermediate and  
260 Silicic Magmas in Deep Crustal Hot Zones, *J. Petrol.*, 47(3): 505-539.
- 261 Arculus, R. and K. Wills (1980), The petrology of plutonic blocks and inclusions  
262 from the Lesser Antilles island arc, *J. Petrol.*, 21(4), 743-799.
- 263 Christensen, N.I. and W.D. Mooney (1995), Seismic velocity structure and  
264 composition of the continental crust: A global view, *J. Geophys. Res.*, 100(B6), 9761-  
265 9788.
- 266 Christensen, N.I. (1979), Compressional wave velocities in rocks at high temperatures  
267 and pressures, critical thermal-gradients, and crustal low-velocity zones, *J. Geophys.*  
268 *Res.*, 84(B12), 6849-6857.
- 269 Christeson, G.L., P. Mann, A. Escalona, T.J. Aitken (2008), Crustal structure of the  
270 Caribbean-northeastern South America arc-continent collision zone, *J. Geophys. Res.*,  
271 113(B8), B08104, doi: 10.1029/2007JB005373.
- 272 Devine, J.D., M.D. Murphy, M.J. Rutherford, J. Barclay, R.S.J. Sparks, M.R. Carroll,  
273 S.R. Young, J.E. Gardner (1998), Petrologic evidence for pre-eruptive pressure-  
274 temperature conditions, and recent reheating, of andesitic magma erupting at the  
275 Soufriere Hills Volcano, Montserrat, WI, *Geophys. Res. Lett.*, 25(19), 3669-3672.
- 276 Donaldsson, C.H. (1977), Laboratory duplication of comb layering in the Rhum  
277 pluton, *Min. Mag.*, 41, 323-336.
- 278 Elsworth, D., G. Mattioli, J. Taron, B. Voight (2008), Implications of Magma  
279 Transfer Between Multiple Reservoirs on Eruption Cycling, *Science*, 322(5899), 246-  
280 248, doi: 10.1126/science.1161297.

281 Shalev, E. et al. (this volume), 3-D Seismic Velocity Tomography of Montserrat From  
282 the SEA-CALIPSO Offshore/Onshore Experiment. *Geophys. Res. Lett.*, Special  
283 Section on Montserrat.

284 Hacker, B. and G. Abers (2004), Subduction Factory 3: An Excel worksheet and  
285 macro for calculating the densities, seismic wave speeds, and H<sub>2</sub>O contents of  
286 minerals and rocks at pressure and temperature, *Geochem. Geophys. Geosyst.*, 5,  
287 Q01005, doi: 10.1029/2003GC000614.

288 Harford, C.L. and R.S.J. Sparks (2001), Recent remobilisation of shallow-level  
289 intrusions on Montserrat revealed by hydrogen isotope compositions of amphiboles,  
290 *Earth Planet. Sci. Lett.*, 185(3-4), 285-297.

291 Harford, C.L., M.S. Pringle, R.S.J. Sparks, S.R. Young (2002), The volcanic  
292 evolution of Montserrat using <sup>40</sup>Ar/<sup>39</sup>Ar geochronology, in *The eruption of the*  
293 *Soufriere Hills Volcano, Montserrat, from 1995 to 1999*, edited by Druitt, T. H. and  
294 B.P. Kokelaar (eds), Geological Society, London, Memoir 21, pp. 93-113.

295 Leake, B.E., et al. (1997), Nomenclature of amphiboles: report of the subcommittee  
296 on amphiboles of the international mineralogical association, commission on new  
297 minerals and mineral names, *The Can. Mineral.*, 35, 219-246.

298 Mattioli, G. S., T. H. Dixon, F. Farina, E. S. Howell, P. E. Jansma, A. L. Smith  
299 (1998), GPS measurement of surface deformation around Soufriere Hills volcano,  
300 Montserrat from October 1995 to July 1996, *Geophys. Res. Lett.*, 25(18), 3417-3420.

301 Murphy, M., S. Loughlin, J. Devine, S. Sparks (1998), The role of magma mixing in  
302 triggering the current eruption at the Soufriere Hills volcano, Montserrat, West Indies,  
303 *Geophys. Res. Lett.*, 25(18), 3433-3436.

304 Paulatto, M., et al. (2009), Upper crustal structure of an active volcano from  
305 refraction/reflection tomography, Montserrat, Lesser Antilles, *Geophys. J. Int.*, in  
306 press.

307 Rudnick, R.L. and D.M. Fountain (1995), Nature and composition of the continental  
308 crust: a lower crustal perspective, *Rev. Geophys.*, *33*, 267-309.

309 Sevilla, W., C. J. Ammon, and B. Voight (subjudice), Crustal Structure Beneath the  
310 Montserrat Region of the Lesser Antilles Island Arc, *Geophys., Geochem., Geosyst.*

311 Sparks, R.S.J., S. Young, J. Barclay, E. Calder (1998), Magma production and growth  
312 of the lava dome of the Soufrière Hills Volcano, West Indies: November 1995 to  
313 December 1997, *Geophys. Res. Lett.*, *25*(18), 3421-3424.

314 Tatsumi, Y., H. Shukuno, K. Tani, N. Takahashi, S. Kodaira, T. Kogiso (2008),  
315 Structure and growth of the Izu-Bonin-Mariana arc crust: 2. Role of crust-mantle  
316 transformation and the transparent Moho in arc crust evolution, *J. Geophys. Res.*, *113*,  
317 B02203, doi: 10.1029/2007JB005121.

318 Watt, J.P., G.F. Davies, and R.J. O'Connell (1976), The elastic properties of  
319 composite materials, *Rev. Geophys.*, *14*(4), 541-563.

320 Westbrook, G.K. and W.R. McCann (1986), Subduction of Atlantic lithosphere  
321 beneath the Caribbean, in *The Geology of North America*, edited by Vogt, P.R. and  
322 Tucholke, B.E., The Western North Atlantic Region, vol. M, The Geological Society  
323 of America, p.341–350.

324 Wyllie, M., A. Gregory and G. Gardner (1958), An experimental investigation of  
325 factors affecting elastic wave velocities in porous media, *Geophysics*, *23*(3), 459-493.

326 Zellmer, G.F., C.J. Hawkesworth, R.S.J. Sparks, L.E. Thomas, C.L. Harford, T.S.  
327 Brewer, S.C. Loughlin (2003a), Geochemical evolution of the Soufriere Hills  
328 volcano, Montserrat, Lesser Antilles volcanic arc, *J. Petrol.*, *44*(8), 1349-1374.

329

329 **Figure Captions**

330 Figure 1. SEM images of a. diktytaxitic mafic magmatic inclusion, b. hypabyssal-  
331 textured noritic anorthosite c. hornblende-gabbro xenolith with adcumulate texture, d.  
332 crescumulate clinopyroxene at boundary of pyroxene-anorthosite layer  
333 (pl=plagioclase, hb=hornblende, px=pyroxene, mg=titanomagnetite, black=vesicles).

334

335 Figure 2. The effect of porosity on estimated compressional wave velocities. Average  
336 velocities of each rock type are plotted with error bars corresponding to the range of  
337 vesicle contents.

338

339 Figure 3. Compressional wave velocities derived from a. estimates based on mineral  
340 proportions, and b. laboratory measurements of similar rocks (Christensen and  
341 Mooney, 1995; see Table 1 for details). Seismic velocity profiles obtained from the  
342 SEA CALIPSO project are also shown (Paulatto et al., in press; Sevilla et al.,  
343 subjudice).

344

344 **Table 1:** Vesicle-free mineral proportions, calculated compressional wave velocities  
 345 and laboratory velocity measurements of the main rock types.

Rock type	Mineral proportions (%)						Velocity estimates (km/s)			Velocity Measurements <sup>a</sup> (km/s)
	plg	hb	opx	cpx	ox.	qtz	Voigt	Ruess	Hill	
<b>Hb-gabbro</b>	58-72	21-38	0-6	0-1	2-4	0	6.84-6.96	6.67-6.74	6.75-6.85	7.10±0.25 <sup>b</sup>
<b>Noritic and gabbroic anorthosites</b>	70-86	0	2-20	0-13	2-8	0	6.80-7.01	6.63-6.69	6.72-6.83	6.89±0.21 <sup>c</sup>
<b>Quartz diorite</b>	69-70	12-15	4-6	0	1-2	7-12	6.69-6.79	6.46-6.54	6.57-6.67	6.44±0.17 <sup>d</sup>
<b>Plagioclase-hornblendite</b>	17	83	0	0	0	0	7.08	7.01	7.05	7.11±0.04 <sup>e</sup>
<b>Plagioclase-clinopyroxenite</b>	14-16	0	2	79-81	3	0	7.58-7.60	7.43-7.45	7.51-7.52	7.71±0.11 <sup>f</sup>
<b>Andesite</b>	73-89	0-5	2-7	1-2	3-8	minor	6.76-6.90	6.58-6.60	6.68-6.74	5.43±0.28
<b>Mafic Inclusion</b>	65	5-28	2-8	2-16	3-6	0	6.98-7.13	6.81-6.83	6.89-6.98	5.88±0.55 <sup>g</sup>

346

<sup>a</sup> Measured at pressure equivalent to 5km depth (Christensen and Mooney, 1995)

<sup>b</sup> Gabbro-norite-troctolite

<sup>c</sup> Anorthosite

<sup>d</sup> Diorite

<sup>e</sup> Hornblendite

<sup>f</sup> Pyroxenite

<sup>g</sup> Basalt

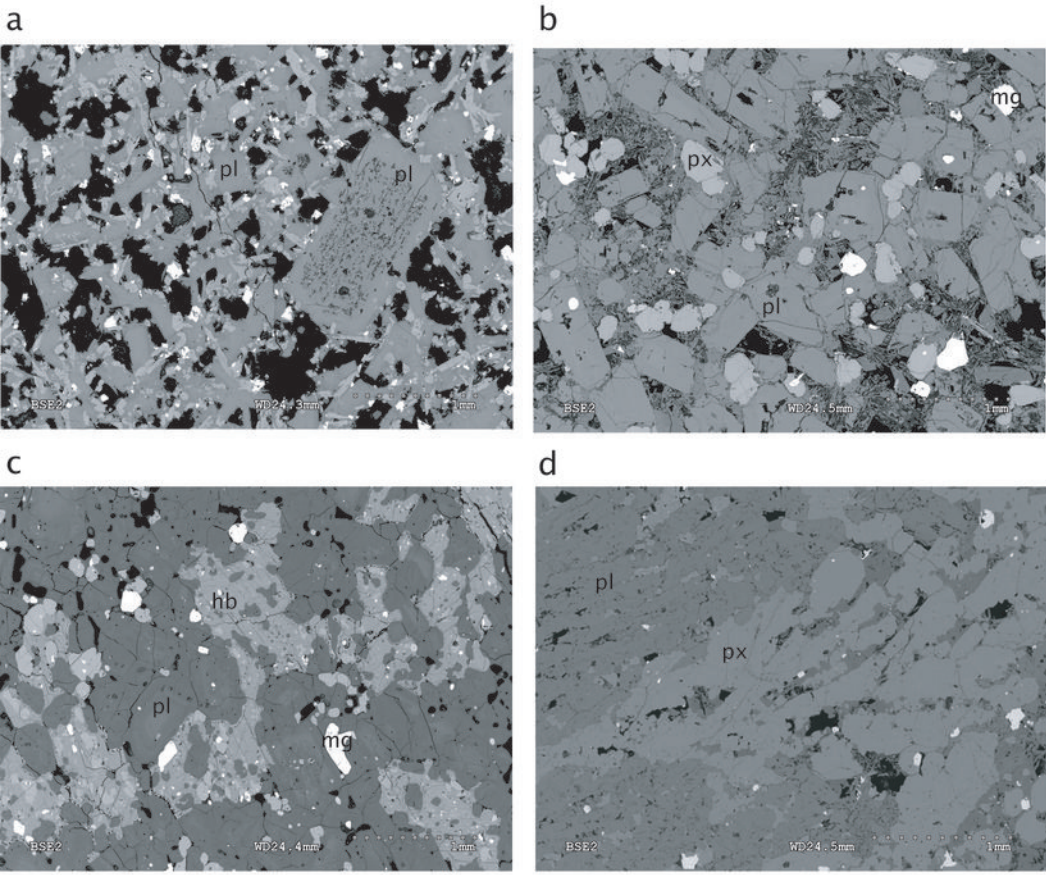


**Figure 1.** SEM images of a. diktytaxitic mafic magmatic inclusion, b. hypabyssal-textured noritic anorthosite, c. hornblende-gabbro xenolith with adcumulate texture, d. crescumulate clinopyroxene at boundary of pyroxene-anorthosite layer (pl=plagioclase, hb=hornblende, px=pyroxene, mg=titanomagnetite, black=vesicles).

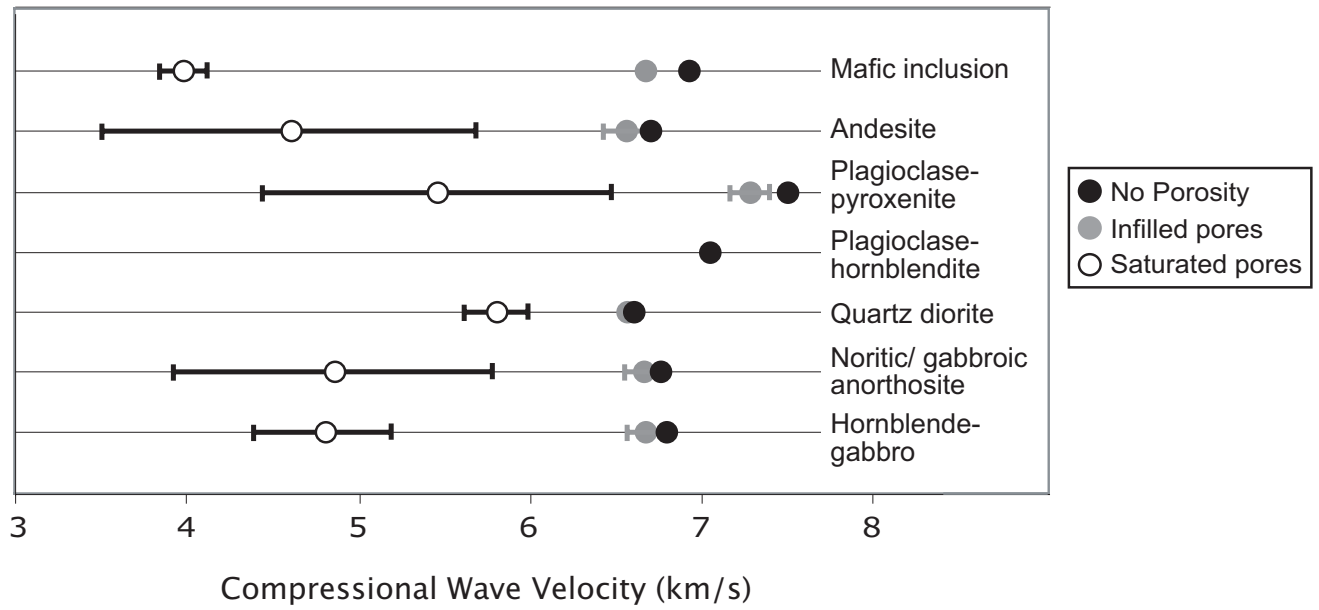


**Figure 2.** The effect of porosity on estimated compressional wave velocities. Average velocities of each rock type are plotted with error bars corresponding to the range of vesicle contents.

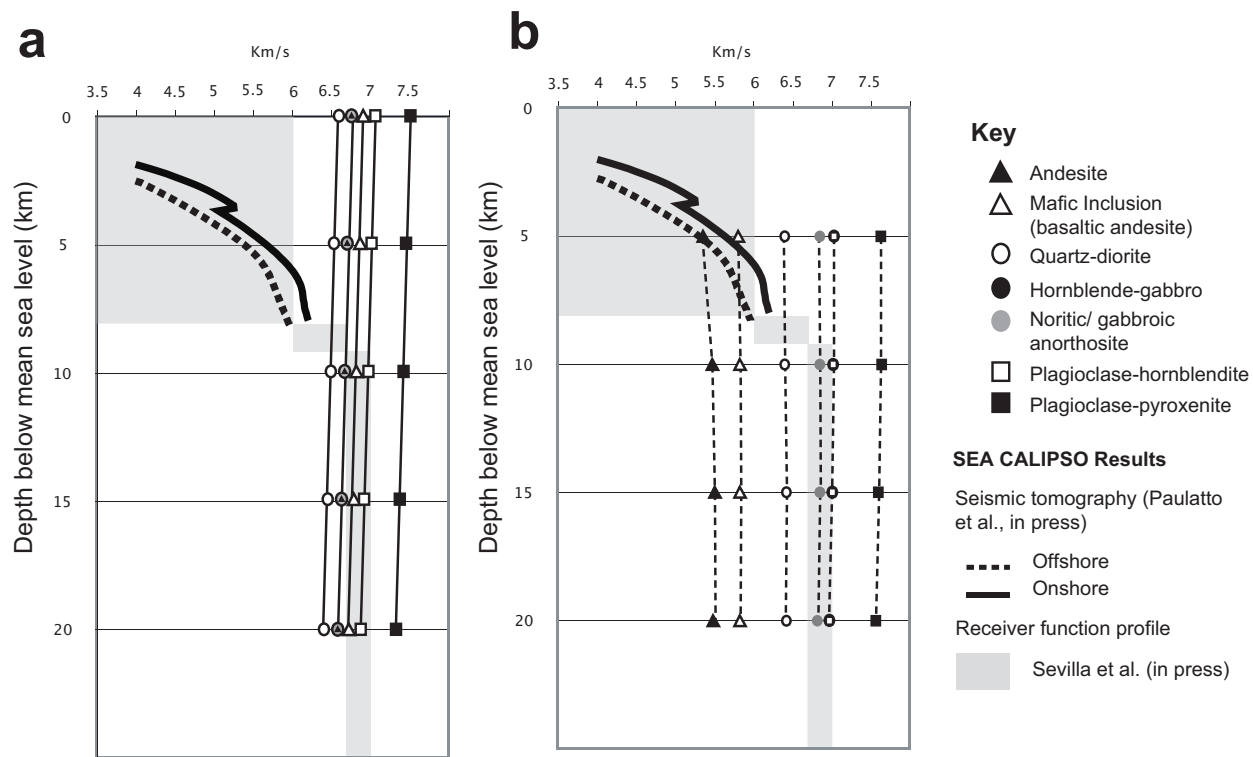


**Figure 3.** Compressional wave velocities derived from a. estimates based on mineral proportions, and b. laboratory measurements of similar rocks (Christensen and Mooney, 1995; see Table 1 for details). Seismic velocity profiles obtained from the SEA CALIPSO project are also shown (Paulatto et al., in press; Sevilla et al., subjudice).